Journal of Volcanology and Geothermal Research 444 (2023) 107944

Contents lists available at ScienceDirect

Journal of Volcanology and Geothermal Research

journal homepage: www.journals.elsevier.com/journal-of-volcanology-and-geothermal-research

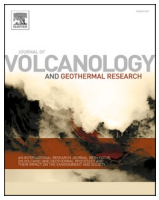

Volcanic harmonic tremor location

Fidencio A. Nava [a], Lenin Ávila-Barrientos [a,b,*], Juan M. Espíndola [c], Francisco J. Núñez-Cornú [d]

[a] Departamento de Sismología, Centro de Investigación Científica y de Educación Superior de Ensenada, Carretera Tijuana-Ensenada 3918, Ensenada, Baja California 22860, Mexico
[b] Direccion Adjunta de Desarrollo Científico, CONAHCYT, Av. Insurgentes Sur 1582, Col. Crédito Constructor, Alcaldía Benito Juárez, 03940 Ciudad de Mexico, Mexico
[c] Departamento de Volcanología, Instituto de Geofísica, Universidad Nacional Autónoma de México, Cd. Mexico 04510, Mexico
[d] C.A. Sismología y Volcanología de Occidente (SisVOc), Puerto Vallarta, Jal. 48280, Mexico

ARTICLE INFO

Keywords:
Volcanic harmonic tremor
Location
Fourier phase
Popocatépetl volcano

ABSTRACT

We present a new method for location of the source of volcanic harmonic tremor, that employs the Fourier phases of an observed tremor segment recorded at various seismic stations, a condition on the inferred phase at the source, and a search location scheme. We discuss the assumptions and limitations inherent to the proposed method. As an illustration of application to real data, the method is used to locate twenty sources of harmonic tremor occurred at Popocatépetl volcano (Mexico) during the July 2006 tremor episode; the located sources agree quite well with results from other studies of seismicity in this volcano.

1. Introduction

Seismic activity is a constant companion of volcanic activity, so its observation and analysis have become the backbone of volcano monitoring. A variety of signals arise from the various processes occurring during the transfer of magma from its sources to the surface, and classification of these signals was the first task carried out by the early volcano seismologists. Today, after more than a century of observations and developments in instrumentation and analysis methods, a classification of volcanic signals has been developed based on their waveforms and spectral characteristics. Seismic events of volcanic origin are now classified under the broad categories of short period (SP), long period (LP) (Chouet, 2003) and, more recently, very long period events (VLP) (Neuberg et al., 1994; Rowe et al., 1998). Among the VLP events, two types of signals are recognized: discrete events and volcanic tremor; the last formally defined as a persistent signal that can last from minutes to several days and is observed only near active volcanoes (Konstantinou and Schlindwein, 2003). Some authors consider these two types of events in the same category because they share similar spectral characteristics and, in some cases, tremor has been considered as a succession of single LP events producing a continuous signal. Other researchers, however, consider them separately from the discrete events arguing that the driving forces are likely different (McNutt, 2005).

Various processes have been proposed to explain the source mechanism of volcanic tremor, most of them involve the hydrodynamics of volcanic fluid of diverse composition, the brittle fracture of melt, or shearing during near-vent extrusion of spines and plugs (e.g. Hellweg, 2000; Julian, 1994; Konstantinou and Schlindwein, 2003; Lees et al., 2004; Chouet and Matoza, 2013, and references therein). Because of the close association between this type of events and magma movement, tremors are significant to volcano monitoring.

Location of the source of volcanic tremor is of fundamental importance, not only to develop models of its generation, but also to contribute to the knowledge about the internal state of an active or erupting volcano, and therefore to be of use as a forecasting tool, given that relations between tremor characteristics and lava output have been proposed (Battaglia et al., 2005), and tremor has been observed to migrate before eruptions (Ogiso and Yomogida, 2012; Ogiso et al., 2015).

Yet, the location of the tremor source has been a challenging problem in volcano seismology because, unlike HF, the tremor signals lack well-defined impulsive arrivals. Thus, alternative techniques have been developed to achieve the location of the tremor source using other properties of the recorded signals. Among these, the following can be mentioned: the method of semblance (coherency from correlation among multichannel data, thence times plus a search for sources that result in best correlation) (Furumoto et al., 1990, 1992); the frequency-slowness method (Goldstein and Chouet, 1994; Chouet et al., 1997);

* Corresponding author at: Departamento de Sismología, Centro de Investigación Científica y de Educación Superior de Ensenada, Carretera Tijuana-Ensenada 3918, Ensenada, Baja California 22860, Mexico.
E-mail address: lenavila@cicese.mx (L. Ávila-Barrientos).

https://doi.org/10.1016/j.jvolgeores.2023.107944
Received 20 February 2023; Received in revised form 5 October 2023; Accepted 24 October 2023
Available online 26 October 2023

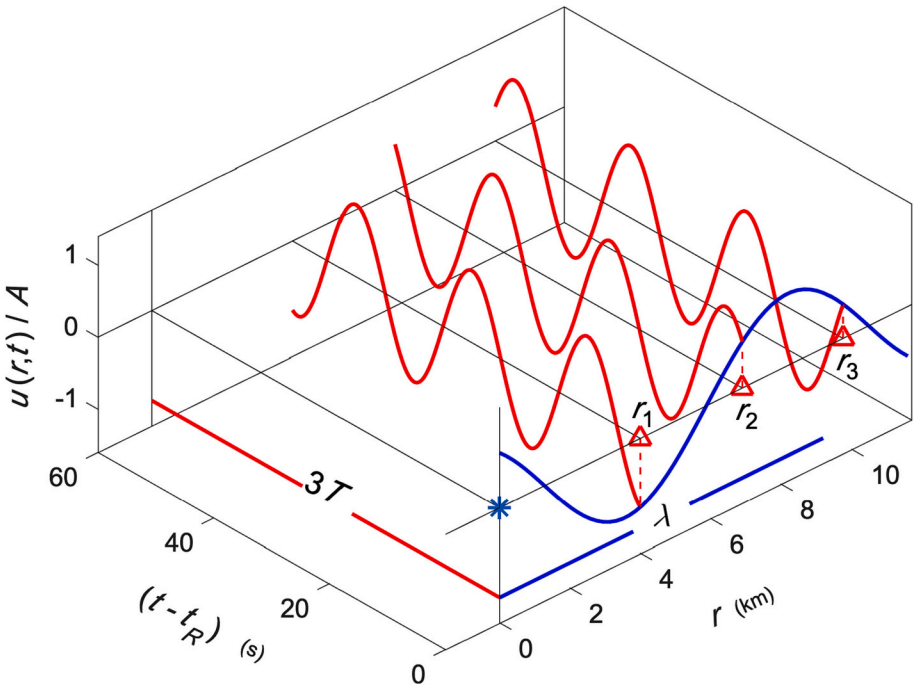

Fig. 1. Traveling vertical wave with wavelength λ (blue curve), originating from a source at the origin (asterisk) and reaching stations (red triangles) so that at a given time t_R, their different phases depend on the distance r. The motion at each station over time is represented by each of the red curves; the Fourier transform of the time series corresponding to these motions yields the phases at t_R. (For interpretation of the references to colour in this figure legend, the reader is referred to the web version of this article.)

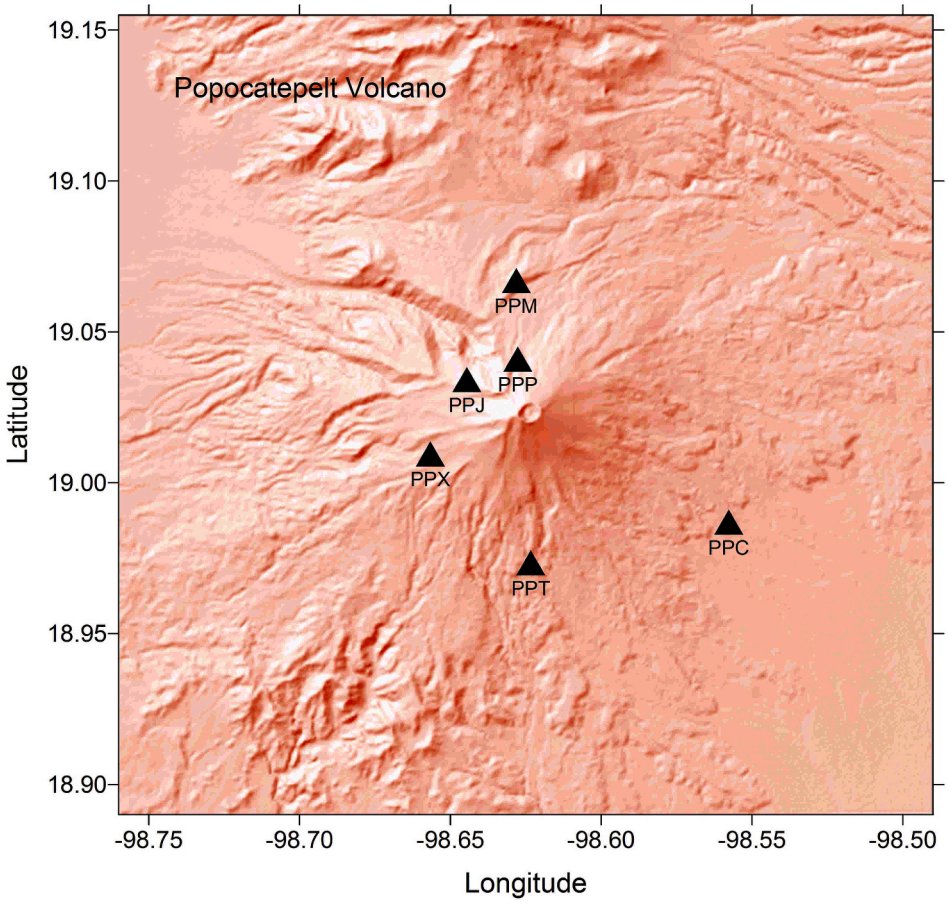

Fig. 2. Seismic stations (black triangles) operating on the Popocatépetl volcano.

Table 1
Seismic stations coordinates, geographical and Cartesian referred to the crater at 98.6271°N and 19.0197°W, and elevations above mean sea level (amsl).

Station	Latitude	Longitude	X	Y	Elevation
	°N	°W	km	km	km amsl
PPC	18.98689714	98.55771124	6.97581	−4.06401	2.670
PPJ	19.03420000	98.64446000	−2.15033	1.16801	4.371
PPM	19.06705867	98.62815300	−0.43480	4.80243	4.009
PPP	19.04103386	98.62760600	−0.37725	1.92389	4.313
PPT	18.97343000	98.62334000	0.07154	−5.55356	3.138
PPX	18.98689714	98.55771124	−3.43934	−1.55561	3.990

distance dependence of signal power and a grid search (Gottschämmer and Surono, 2000); 3D grid search using the amplitude decay of the seismic signal (Di Grazia et al., 2006; Ogiso et al., 2015; Ogiso and Yomogida, 2020); spatial contours of seismic amplitudes corrected for station site effects (e.g. Battaglia and Aki, 2003; Battaglia et al., 2003; Battaglia et al., 2005; Kumagai et al., 2010, 2019); interstation arrival times computed using cross correlation of waveforms (e.g. Haney, 2010; Droznin et al., 2015; Li et al., 2017), some of them complemented with back azimuths from wave directions (Métaxian and Lesage, 1997; Métaxian et al., 2002); double-correlation of analytic signals (Li et al., 2017); correlation of waveform envelopes (Yukutake et al., 2017); eigenvalues from cross-correlation matrices (Soubestre et al., 2019; Maher et al., 2023); source grid search to look for beam-forming (Wassermann, 1997), approximate provenance direction estimation from particle motion (Arámbula-Mendoza, 2002; Arámbula-Mendoza and Valdéz-González, 2002). A somewhat similar problem is location of non-volcanic tremor, which is mainly done by cross correlation and beam forming (e.g. Shelly et al., 2006; Wech and Creager, 2008).

Most of the above-mentioned methods result in very approximate locations of the tremor sources and some of them require dense seismograph arrays (Chouet et al., 1997; Rost and Thomas, 2002). Yet volcanic tremor is an important feature of volcanic activity, which must be analyzed if an understanding of its origin and use as a forecasting tool are to be achieved. Thus, it is opportune to add new methods of location to the volcanologist toolbox, given that a new, independent tool can complement existing ones and help reduce uncertainty.

In this work, we present a new method for locating harmonic tremor, and illustrate its application to real data by locating sources of harmonic tremor that occurred at Popocatépetl volcano, central Mexico, during a tremor episode in 2006.

2. Method

The method proposed here is applicable to volcanic harmonic tremor, defined as sustained tremor having multiple peaks in the spectrum with a fundamental frequency plus its harmonics (Konstantinou and Schlindwein, 2003), nice examples of tremors featuring several harmonics are shown in Almendros et al. (2014) and Roman (2017). We consider monochromatic tremor having a single spectral peak to be a particular case of harmonic tremor. In what follows, harmonic, including monochromatic, tremor will be simply referred to as tremor.

2.1. Premises

a) Tremor has a localized source, i.e. a source with spatial dimensions small enough to be modeled adequately as a point in space with respect to the overall dimensions of the observation network and the volcano itself. Tremor with multiple dominant frequencies may have a different source for each one. This premise is supported by the argument that, if there were not a localized source and the whole edifice were vibrating as a whole, then signals at all stations would all have essentially (apart from noise disturbances) the same Fourier phase for each frequency, which is definitely not so for observed cases.
b) The seismic signal propagates from the source with radial symmetry.
c) The average seismic velocity in the medium between the source and the observation points (stations) can be adequately represented by a constant value. An average velocity that varies according to the azimuth and the relative positions of the stations with respect to the source could be implemented, but volcano velocity structures are mostly unknown, so the added complexity of variable average velocities is not justified.

These premises are used in many of the above-mentioned tremor locating methods. However, how adequate our premises are will be measured by the results of the application of the method.

2.2. Theory

Let there be a standing tremor oscillation originating at some point $h_0 = (x_0, y_0, z_0)$, and propagating through the volcano with velocity v, then at time t the Fourier component of the (vertical) motion, corresponding to frequency f_o, at the source can be represented as

$$u_0(t) = cos[2\pi f_o(t - t_R) + \phi_0] \quad (1)$$

where t_R is a reference time and ϕ_0 is the source phase at t_R for that particular frequency (Fig. 1).

At a seismic station located at $h_i = (x_i, y_i, z_i)$, a distance $r_i = \sqrt{(x_i - x_0)^2 + (y_i - y_0)^2 + (z_i - z_0)^2}$ from the source, the corresponding spectral component for frequency f_o is

$$u_i(t) = cos[2\pi f_o(t - t_R) + \phi_0 + 2\pi r_i/\lambda] = cos[2\pi f_o(t - t_R) + \phi_i], \quad (2)$$

where $\lambda = v/f_o$ is the wavelength (Fig. 1), ϕ_i is the phase at station i referred to t_R and is related to ϕ_0 as

$$\phi_0 = \phi_i - 2\pi r_i/\lambda. \quad (3)$$

In order to estimate ϕ_i, $i = 1, 2, \ldots, N_S$, where N_S is the number of stations, from a segment of the observed data time series for which a particular frequency of interest, f_o, is constant at all stations, a section spanning an integer number of periods $T = 1/f_o$ is chosen. Let the initial and ending times of the section be t_R, $t_R + kT$, where k is an integer (as large as possible) so that the discrete Fourier transform (DFT) can evaluate the f_o component exactly.

The measured phase at station r_i, referred to t_R, is estimated from the DFT spectrum of the observed motion, $U_i(f)$, as

$$\widehat{\phi}_i = tan^{-1}\left(\frac{Im\ U_i(f_o)}{Re\ U_i(f_o)}\right) - \Delta\phi_i\ (f_o), \quad (4)$$

where $\Delta\phi_i\ (f_o)$ is the phase shift introduced by the measuring instrument, which may include the $-i$ shift resulting from integration of velocity records; if all instruments have the same response, then the instrumental phase shift can be ignored.

Since the arctan function cannot distinguish between phases differing by an integer number of 2π, the phases given by (4) are "wrapped" and the phase at the source, estimated from $\widehat{\phi}_i$ is related to the measured one as

$$\widehat{\phi}_{0i} = \widehat{\phi}_i - 2\pi\ r_i/\lambda + n_i 2\pi; n_i \in \mathbb{Z}. \quad (5)$$

This n_i uncertainty is not an insurmountable problem for two reasons: first, because in the genetic location scheme described below, for each trial source that results in some trial source-receiver distance r_i the appropriate n_i can be estimated as

$$n_i = \lfloor r_i/\lambda \rfloor; \quad (6)$$

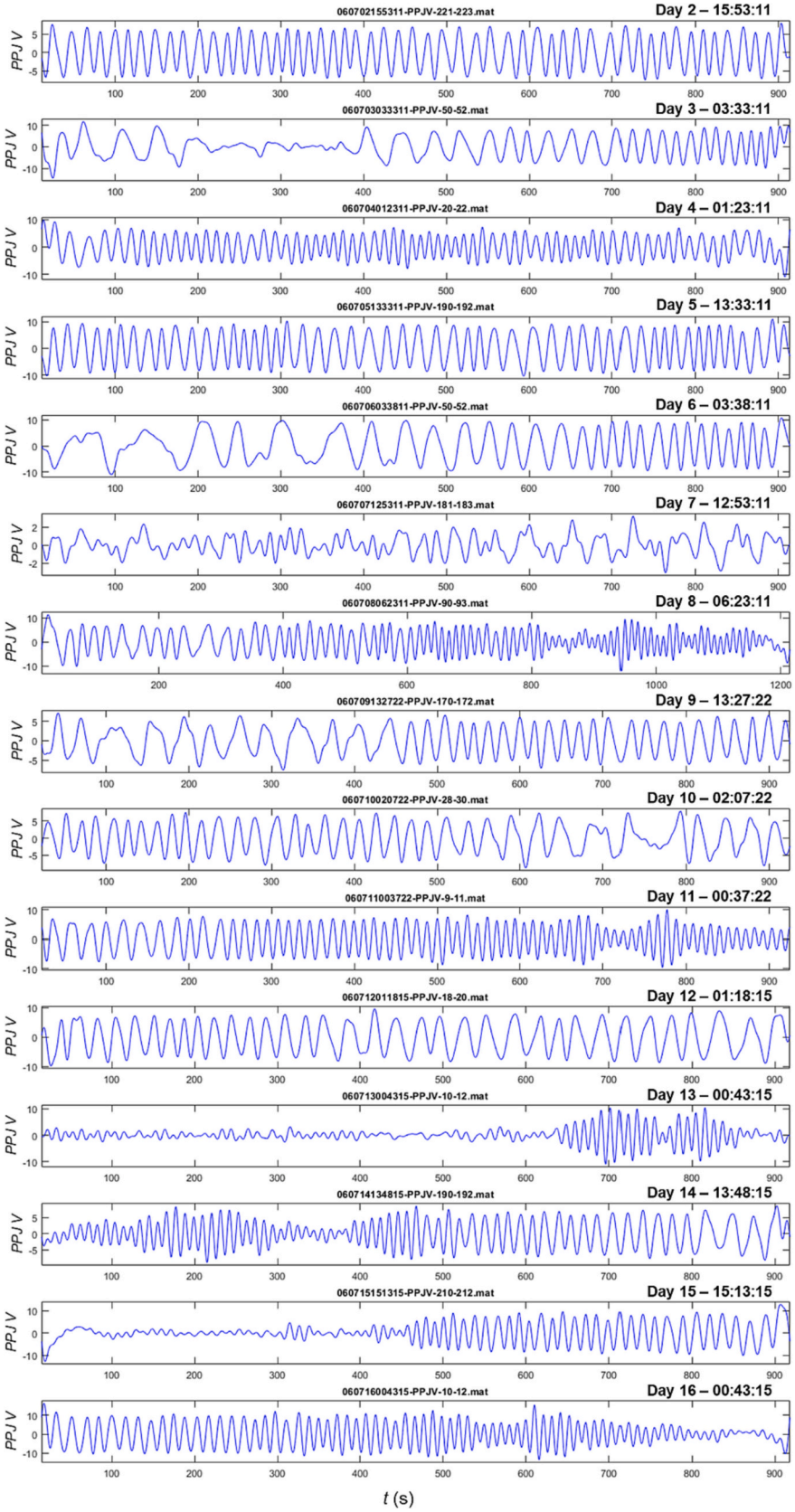

Fig. 3. Tremor waveforms at the PPJ station, from July 2 to July 31, 2006; the day of the month and time for the beginning of each trace are indicated over each plot.

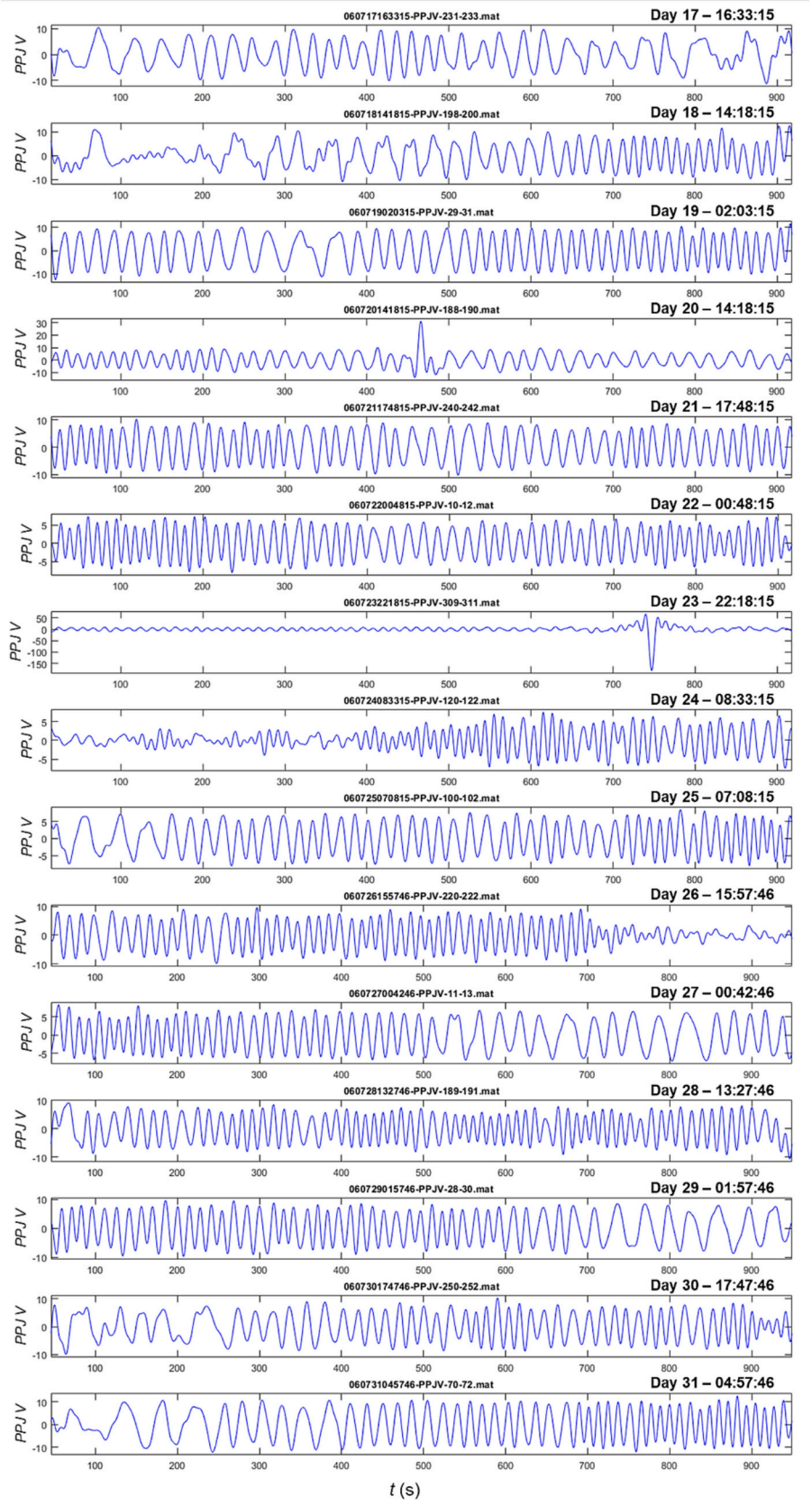

Fig. 3. (*continued*).

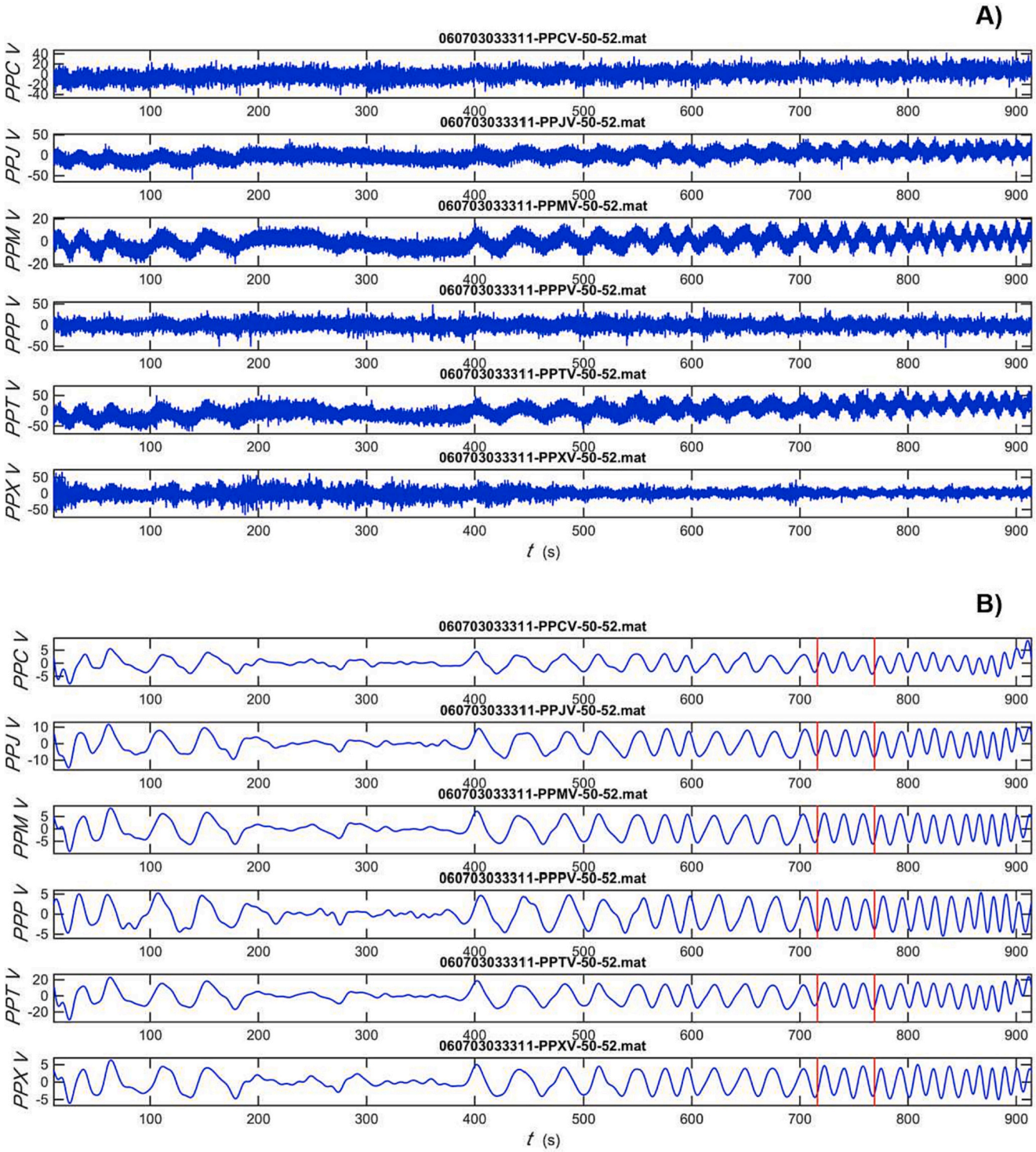

Fig. 4. Observed time series 15.05 min long segment unfiltered (A) and bandpass filtered (B). Vertical lines in (B) delimit the segment that was selected for analysis. Times are referred to the date coded above the traces (060703033311 indicates 2006/07/03 03:33:11 UTC). The forms shown are typical of those for most of the observed period.

second, because the frequencies to be used should, whenever possible, be small enough so that $\lambda > r_i \forall i$ and the wrapped phase corresponds to the true one. In what follows, we will assume that any necessary corrections have been made to the measured phases and that $\widehat{\phi}_i$ represents the correct observed phase.

Next, a search (described below) is made to find the optimum combination of h_0 and v that best satisfies Eq. (5) for all stations. Of course ϕ_0 is not known, but, and this is the crux of the matter, we know that it is the same for all stations; in the ideal case, with a truly constant velocity and no noise, the $\widehat{\phi}_{0i}$ estimates from all stations would be equal. For real data the chosen source will be the one that results in the least spread for the $\widehat{\phi}_{0i}$ estimates over all stations, and the standard deviation of these estimates, s_ϕ, is a convenient means of measuring that spread

In order to choose convenient f_o frequencies, a "minimal spectrum" is constructed by choosing for each frequency the minimum absolute value

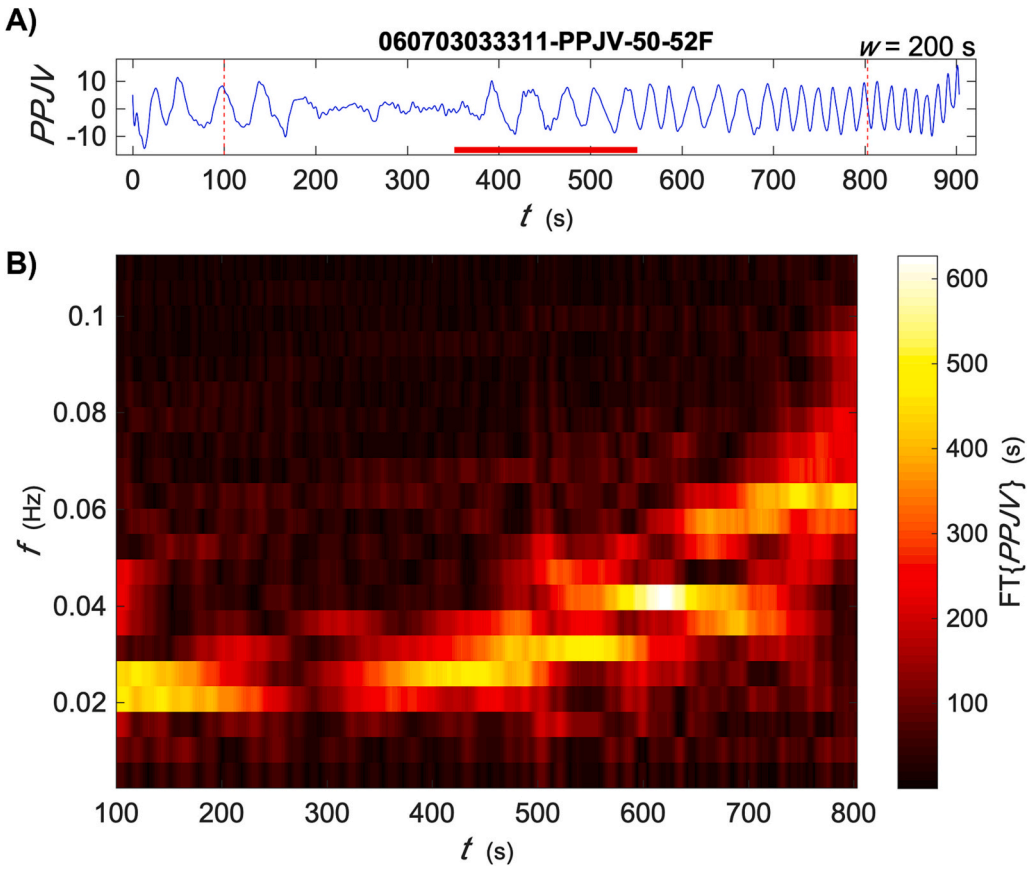

Fig. 5. Spectrogram of the signal at PPJV shown in Fig. 4. (A) Observed, bandpassed signal (blue) the horizontal red line shows the length of the time window used in the spectrogram. (B) Spectrogram with spectral amplitudes colour-coded according to the bar on the right. (For interpretation of the references to colour in this figure legend, the reader is referred to the web version of this article.)

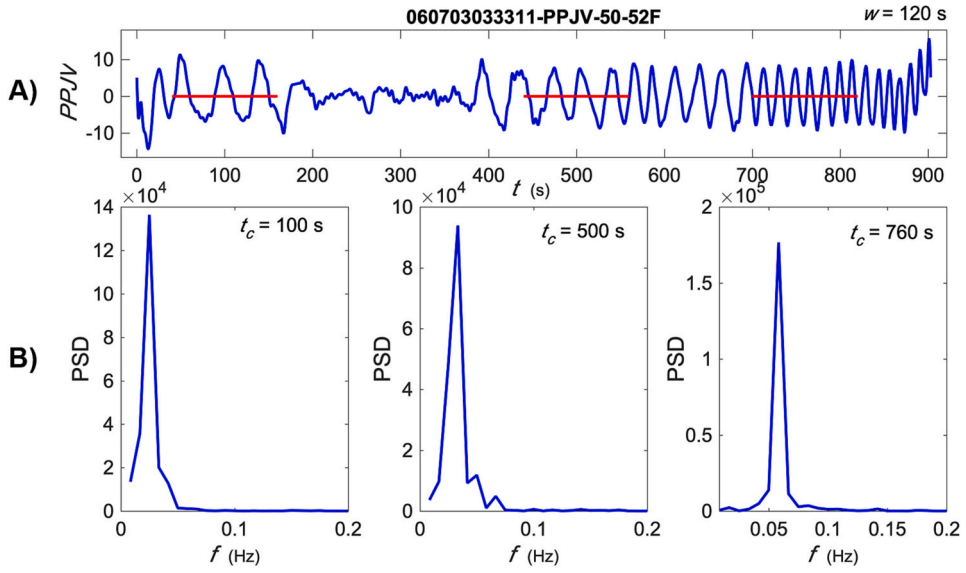

Fig. 6. PSD plots from the signal at PPJV shown in (A) (blue) for three time windows (horizontal red lines) centered at times $t_c = 100$ s (B, left), $t_c = 500$ s (B, center), and $t_c = 760$ s (B, right). (For interpretation of the references to colour in this figure legend, the reader is referred to the web version of this article.)

among all spectra f calculated for the same time interval at all stations, so that significant peaks in the minimal spectrum are sure to have enough energy at all stations.

2.3. Location scheme

For each trial velocity, a search for the corresponding optimum hypocenter, the one resulting in the minimum standard deviation of estimated source phases, is carried out. Next, other trial velocities are tried

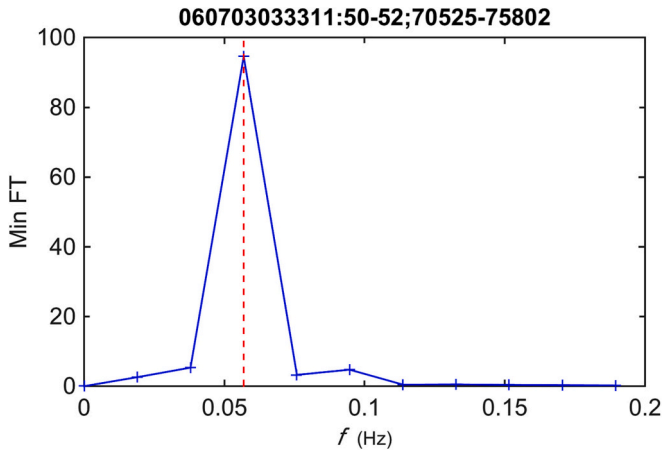

Fig. 7. Minimal spectrum.

to search for a minimum minimorum standard deviation, $s_{\phi min}$, that corresponds to the optimal combination of location and velocity.

The search for the optimum source for a given velocity is, broadly, as follows: starting with a 3D grid of candidate sources, the N_p sources giving the best results, the ones with the smallest spreads in the estimated $\widehat{\phi}_0$, are chosen as parents of the next generation. For each parent source 6 children are generated by varying the parent (x_0, y_0, z_0) values, one at a time positively and negatively, using variations that diminish each generation by a factor close to one. The locations of the children may be anywhere in space, outside or inside the original grid. From among all parents and children the best N_p are chosen as a new generation of parents. The process is iterated until the variations reach a given minimum value. The resulting location is classified as: A (excellent) for $s_{\phi min} \leq 0.05$, B (good) for $0.05 < s_{\phi min} \leq 0.10$, C (approximate) for $0.10 < s_{\phi min} \leq 0.20$, and D (unreliable) for $s_{\phi min} > 0.20$. If, during a search, all children locate outside or above the volcano, then the event is considered unlocatable and discarded.

Table 2
Phase at each station (radians).

Station	$\widehat{\phi}_i$
PPC	2.59031
PPJ	1.84022
PPM	2.312738
PPP	1.502263
PPT	2.287828
PPX	2.276776

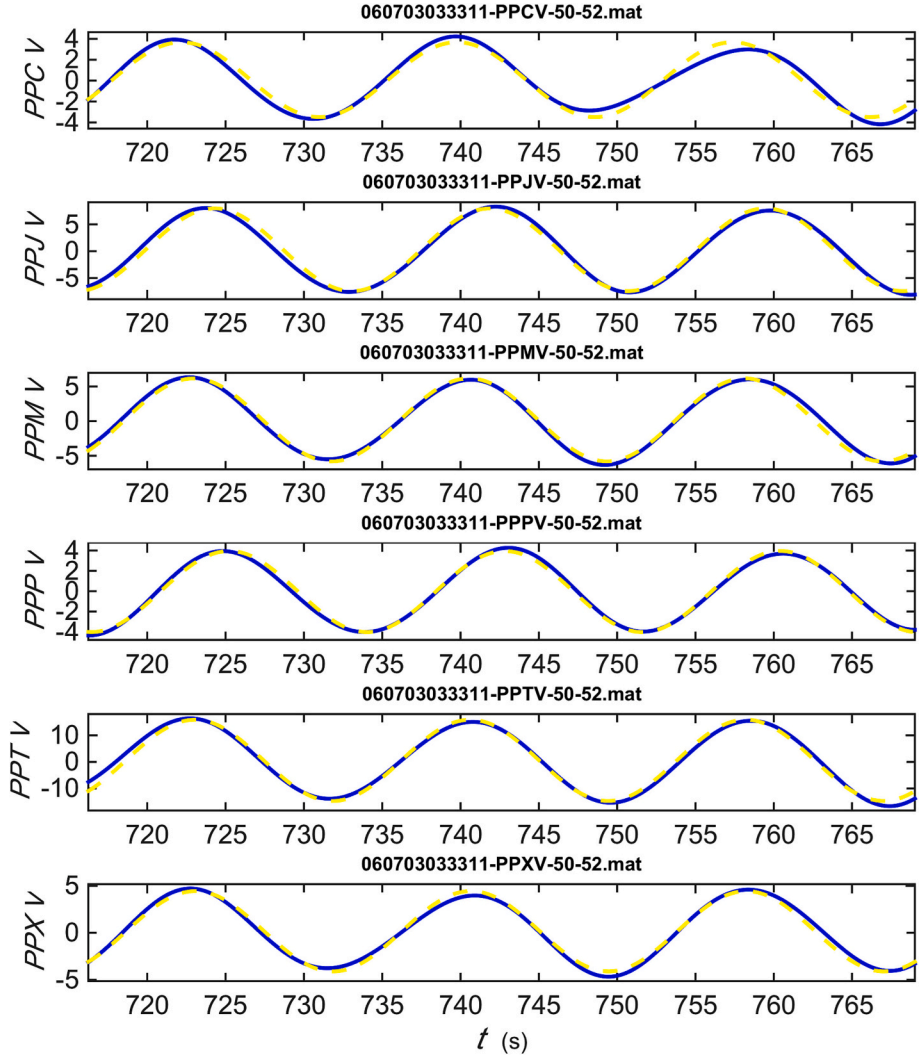

Fig. 8. Selected sections spanning three periods (blue lines) and the corresponding cosines determined from the Fourier phases at each station and the common frequency (dashed yellow). (For interpretation of the references to colour in this figure legend, the reader is referred to the web version of this article.)

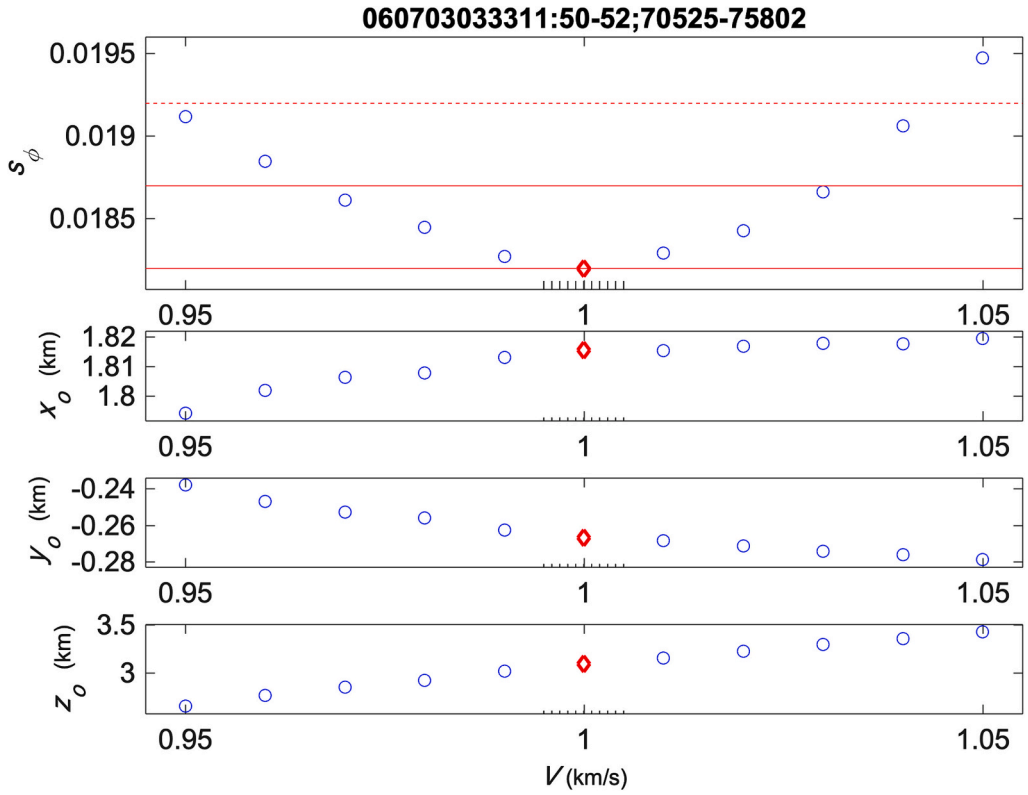

Fig. 9. Velocity search: Source phases standard deviation s_ϕ and source coordinates vs average velocity V. The preferred solution for minimum s_ϕ is indicated by red diamonds, in this example for $V = 1$ km/s. (For interpretation of the references to colour in this figure legend, the reader is referred to the web version of this article.)

The value of $s_{\phi min}$ is a measure of how the $\widehat{\phi}_{0i}$ estimated phases differ from their average $\widehat{\phi}_0$, and can be used together with λ for a rough estimate of uncertainty. However, it is possible to get a better estimate by considering each individual difference $\widehat{\phi}_{0i} - \widehat{\phi}_0$ together with the unit vector from station to hypocenter that indicates in which direction the distance corresponding to this phase difference points. For each axis, the sum of all components of these distances in each direction is a measure of the uncertainty of the location along the axis.

The effects on locations due to the particular instrumental array used in the application will be discussed below.

2.4. Significance and source probability

It is possible to judge how good our supposition of there being a localized source for the harmonic tremor is, i.e. to assess the significance of finding a set of phases that result in a phase determination, by considering the null hypothesis: that there is no localized source so that phases at all stations are randomly distributed with uniform probability over an interval of length 2π.

A first element to use is the ratio

$$R_0 = s_{\phi min} / s_U, \tag{7}$$

where $s_U = 2\pi/\sqrt{12} = 1.8138$ radians is the standard deviation for a uniform distribution over the interval $0 < \phi < 2\pi$ (Battaglia, 2007).

A second element is the probability, under the null hypothesis, of N_S uniformly distributed phases to fall within an interval $\pm q s_{\phi min}$, where q is a constant,

$$p_0 = Pr(N_S \,|s_{\phi min}, q) = \left(\frac{2q s_{\phi min}}{2\pi}\right)^{N_S - 1}. \tag{8}$$

3. Application to real data

In what follows we will illustrate the proposed method by applying it to harmonic tremor recorded during the July 2006 crisis at the Popocatépetl volcano in Mexico. We should point out that the data do not constitute an excellent set: there are only six stations, the azimuthal coverage is not very good, and the observed tremor itself shows changes in the dominant periods (discussed below) that complicate the location process; however, these limitations can be seen as a stringent test on the method, and the physically and geologically reasonable results suggest that the method is valid.

We will show first in detail the application of the method to a good set of seismograms, and afterwards the results for all located hypocenters.

Although, as mentioned above, it is possible to correct for phase wrapping, it is desirable to work with the longest possible periods, since path differences and noise in general introduce time travel variations that result in small phase shifts for long wavelengths, but can produce unacceptably large phase shifts for small wavelengths. In practice, wavelengths should be larger than the largest source-station distance.

The Popocatépetl (Smoking Mountain) volcano is an andesite stratovolcano located in the central part of the Trans-Mexican Volcanic Belt, some 60 km SE of Mexico City (Chouet et al., 2005; Delgado et al., 2008), where the states of Morelos, Puebla and Mexico meet. The Popocatépetl crater is located at 98° 37′ 37.5" W and 19° 01′ 10.98" N, and the 'upper lip' summit is its highest elevation at $z_s = 5.452$ km above mean sea level, making the Popocatépetl the second-highest volcano in Mexico (Arciniega-Ceballos et al., 2003; Cabral-Cano et al., 2008).

The historic activity of Popocatépetl, from 1354 to the present shows many different kinds of eruptive events (De-la Cruz-Reyna et al., 1995; Macías et al., 1995; Siebe et al., 1995; Valdés et al., 1995), including a major Plinian eruption about 822 CE (Siebe et al., 1996). Prehistoric activity includes at least four extremely large avalanches, the youngest

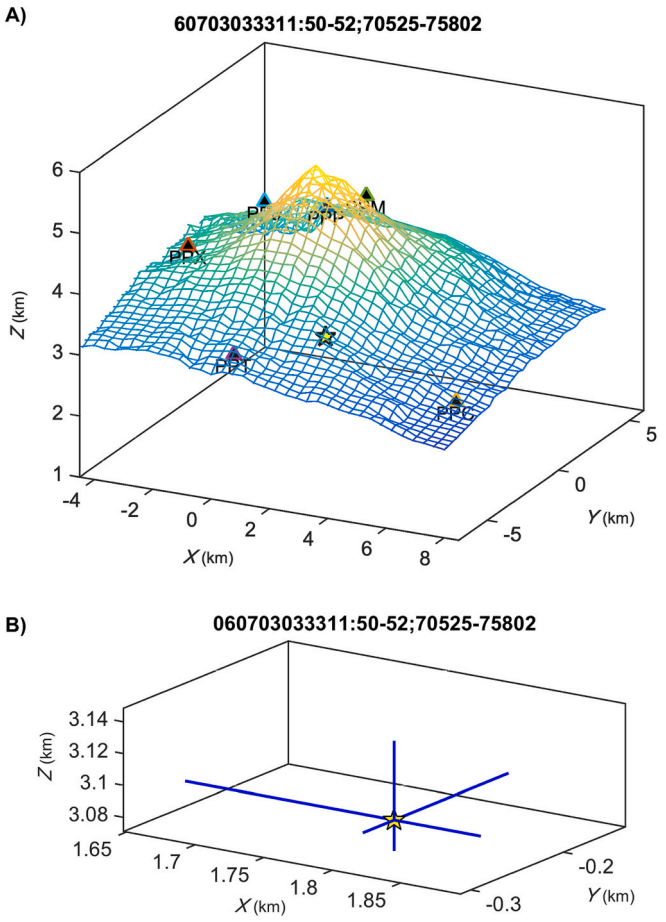

Fig. 10. A) Hypocentral location: triangles are the stations, the circle indicates the position of the crater and the yellow star is the source location. B) Close-up of source: the yellow star indicates the source position and the blue lines are the error bars. (For interpretation of the references to colour in this figure legend, the reader is referred to the web version of this article.)

Table 3
Random occurrence probabilities and confidence levels (Chebychev and Normal) vs. q.

$s_{\phi min} = 0.1048\,\lambda = 15.6292$ km

q	p_0	C. Cheb.	C. Norm.	δr
1	$6.520{\cdot}10^{-12}$	≥ 0.00000	0.10125	
2	$2.086{\cdot}10^{-10}$	≥ 0.17798	0.75623	
3	$1.584{\cdot}10^{-9}$	≥ 0.49327	0.98391	
4	$6.676{\cdot}10^{-9}$	≥ 0.67893	0.99994	

one from some 23,000 years ago (Siebe et al., 1995), so this volcano represents an important hazard for the nearby large cities of Mexico and Puebla (Macías et al., 1995). After the 1919–1938 eruptive period, volcanic activity consisted of mild fumarolic activities that began to increase in 1993 (Chouet et al., 2005), heralding the current activity of Popocatépetl that started on December 21, 1994 (Espíndola et al., 2004; Delgado et al., 2008), and continues to date; a detailed account of the volcano's activity from 1994 to 2011 can be found in the papers contained in CENAPRED (1995), and in Espinasa (2012), and Delgado et al. (2008)

In 2006 a period of enhanced activity started on January 6 with a small explosion, and two explosions that occurred on January 25 and 26 destroyed the 28th dome (Espinasa, 2012). The explosion of January 26 produced a plume about 8.4 km high (http://volcano.si.edu). From March 6 to May 8 the volcano presented several harmonic tremor episodes. On April 12 and May 23 the volcano had two explosions followed by spasmodic tremor, which produced two plumes with low ash content and <2 km high (Espinasa, 2012).

Between July 2 and July 31, 2006 the volcano presented an episode of harmonic tremor, which we are using to illustrate our location method. During this time, on July 25, an explosion that generated a 5 km high ash plume followed by spasmodic tremor.

Fig. 2 shows the topography of the Popocatépetl volcano, and the seismographic stations operated by the *Centro Nacional de Prevención de Desastres* (CENAPRED). Table 1 shows the station coordinates and elevations. The seismographs are triaxial Mark L-4C-3D instruments with 1.0 Hz natural frequency and sampling interval $\Delta t = 0.01$s.

Samples of observed tremor (Fig. 3) for each day, from July 2 to July 31, show that the signals observed locally were due to volcanic unrest and not to some teleseismic source, active off and on during a whole month, that would have been recorded at stations away from the volcano. All signals have been bandpass filtered from 0.01 Hz to 0.1 Hz, as illustrated in Fig. 4. Although there are many instances of harmonic tremor in the 0.1 to 7 Hz range (e.g. Konstantinou and Schlindwein, 2003) and Popocatépetl has exhibited tremor in this range (e.g. Arámbula-Mendoza et al., 2016; Roman, 2017), during the July 2006 episode tremor occurred in the 0.01 to ~0.15 Hz range with durations of tens of minutes.

Most of the July 2006 tremors are predominantly monochromatic, with only a few instances of at most two harmonics, and they all exhibit strong frequency gliding in time, both towards higher and lower frequencies. This frequency gliding, dominant frequency changing with time, has been observed at several volcanoes where it is sometimes related to explosions (Lesage et al., 2006; Maryanto et al., 2008; Hotovec et al., 2013; Eibl et al., 2015; Unglert and Jellinek, 2015).

The main problem we encountered when locating tremor sources for the July 2006, crisis at Popocatépetl volcano, was due to the frequency gliding, because dominant frequencies changed quite rapidly with time (Figs. 3 and 4), so it was very difficult to obtain samples having the same dominant frequency over more than two cycles.

3.1. Detailed example: July 3, 2006

Fig. 4, shows seismograms for July 3, 2006. It can be seen (top) that tremor appears at all stations with a considerable amount of high-frequency noise. Bandpass filtering, $0.01\text{Hz} \leq f \leq 0.10\text{Hz}$, was applied to eliminate the high-frequency and very-long-period noise.

The filtered signal, in Fig. 4, shows that the dominant period changes in time, and although a section may resemble a train of dispersed surface waves, the persistence of this kind of signals over a whole month (Fig. 3) and different patterns of period changes preclude a teleseismic source, but point to frequency gliding. This frequency gliding was typical of the Popocatépetl's tremor signals over the whole month of activity, and makes it very difficult to sample several cycles having the same the dominant period(s); we found only a few cases of three cycles, and most cases spanned only two cycles. No locations were done for single cycle samples because we considered they would be unreliable.

Fig. 5 shows a spectrogram of the signal at station PPJV shown in Fig. 4, where the gliding in time of the single dominant frequency can be clearly seen.

Fig. 6 shows a power spectral density (PSD) plot for the signal at PPJV shown in Figs. 4 and 5. PSD's measured at three-time windows show the monochromatic character of the signal and the frequency gliding.

From the filtered time series, a segment for which the dominant period is approximately constant is selected (Fig. 3), with length corresponding to an integer number of periods, so that the Fourier transform will be able to correctly evaluate that component. We choose the periods as long as possible, in order to work with wavelengths that are large compared with the source-station distances.

In this example, a section corresponding to three complete cycles,

Table 4
Location coordinates, frequency, preferred velocity, minimum phase standard deviation and probability of phases occurring within $q = 3$ standard deviations by chance.

Date	x_0 (km) ϵ^-/ϵ^+	y_0 (km) ϵ^-/ϵ^+	z_0 (km) ϵ^-/ϵ^+	f_o (Hz)	v (km/s)	$s_{\phi min}$ (rads)	p_0 $(q = 3)$
7/2/2006	1.921 −0.010/+0.065	0.222 −0.073/+0.007	−0.671 −0.072/+0.042	0.0714	0.770	0.00000	5.43E-17
7/3/2006	1.815 −0.151/+0.062	−0.267 −0.032/+0.122	3.095 −0.018/+0.048	0.0568	1.000	0.01820	1.58E-09
7/4/2006	2.205 −0.463/+0.606	0.268 −0.360/+0.174	3.758 −0.096/+0.058	0.0787	1.230	0.10510	1.02E-05
7/4/2006	2.437 −0.058/+0.012	0.472 −0.000/+0.072	0.865 −0.019/+0.048	0.0745	0.850	0.00000	3.15E-16
7/5/2006	1.788 −0.169/+0.168	0.293 −0.077/+0.077	−0.510 −0.217/+0.217	0.0510	0.570	0.08250	3.03E-06
7/5/2006	1.967 −0.266/+0.325	0.407 −0.217/+0.051	−1.962 −0.421/+0.361	0.0544	0.450	0.15140	6.32E-05
7/9/2006	2.531 −0.266/+0.332	0.443 −0.259/+0.160	3.767 −0.055/+0.025	0.0517	0.930	0.05160	2.91E-07
7/10/2006	1.918 −0.143/+0.143	0.385 −0.061/+0.061	−0.513 −0.178/+0.178	0.0585	0.690	0.06500	9.22E-07
7/10/2006	2.423 −0.180/+0.215	0.156 −0.119/+0.064	3.102 −0.062/+0.046	0.0855	1.330	0.04250	1.10E-07
7/11/2006	2.311 −0.148/+0.108	0.279 −0.015/+0.073	3.243 −0.019/+0.035	0.0786	1.520	0.02370	5.96E-09
7/12/2006	1.731 −0.038/+0.013	0.101 −0.008/+0.022	−1.948 −0.034/+0.042	0.0527	0.310	0.01390	3.13E-08
7/15/2006	1.783 −0.447/+0.581	−0.126 −0.328/+0.188	−0.307 −0.595/+0.513	0.0479	0.540	0.17790	0.0001416
7/16/2006	1.506 −0.372/+0.395	−0.234 −0.231/+0.217	−1.165 −0.586/+0.575	0.0714	0.830	0.18620	0.0001779
7/16/2006	1.947 −0.670/+0.671	−0.214 −0.323/+0.322	1.250 −0.520/+0.524	0.0917	1.300	0.21030	0.0003265
7/19/2006	1.790 −0.719/+0.747	−0.201 −0.386/+0.359	0.365 −0.760/+0.744	0.0665	0.940	0.24550	0.0007084
7/19/2006	1.413 −0.537/+0.556	−0.308 −0.341/+0.331	−0.966 −0.833/+0.824	0.0953	1.240	0.24090	0.0006442
7/21/2006	1.910 −0.793/+0.776	−0.210 −0.386/+0.405	−0.202 −0.910/+0.922	0.0726	0.820	0.37400	0.005807
7/22/2006	2.057 −0.038/+0.021	0.035 −0.004/+0.022	−0.595 −0.026/+0.033	0.0759	0.280	0.00520	6.12E-10
7/27/2006	2.241 −0.037/+0.027	0.092 −0.009/+0.033	0.237 −0.026/+0.035	0.0626	0.410	0.01660	6.36E-08
7/31/2006	1.757 −0.460/+0.509	−0.023 −0.265/+0.208	0.024 −0.546/+0.517	0.0620	0.540	0.26250	0.0009899

containing samples with indices from 70,525 to 75,802, was chosen (Fig. 3). From the spectra of these time series, the minimal spectrum, shown in Fig. 7, was used to choose the common period $T = 17.5933$ s ($f = 0.0568$ Hz); the cosine corresponding to this common frequency, adjusted for the spectral amplitude and phase for each station, is shown as the dashed yellow line on top of the observed time series in Fig. 7.

Fig. 8 shows a close-up of the selected segment and the cosine of the common frequency $f_o = 0.0568$ Hz selected from the minimal spectrum with the initial phase determined from the spectrum for each station (Table 2).

Finally, based on the phases for the common frequency $f_o = 0.0568$ Hz at the different stations (Table 2), the tremor source is located, as mentioned above, by trying different average velocities, v, in the location scheme. The initial grid of candidate sources spans from −6 km to 6 km, with 0.25 km spacing in the X and Y directions, and from −1 km to 3.9 km with 0.05 km spacing in the Z direction.

Fig. 9 illustrates the search for the optimal velocity (to 2 decimal places). The upper plot corresponds to the source phase standard deviation for each velocity and shows a clear minimum of $s_{\phi min} = 0.0182$ radians for $v = 1.00$ km/s, which corresponds to a wavelength $\lambda = 17.5933$ km. The three bottom plots in Fig. 9 show the X, Y, and Z coordinates of the hypocenter for each velocity; the X and Y coordinates are kilometers referred to the location of the volcano's crater.

Our preferred location is shown in Fig. 10 by a yellow star, at $x_0 = 1.8155\,[-0.1515/+0.0621]$ km, $y_0 = -0.2668\,[-0.0325/+0.1223]$ km from the crater, and $z_0 = 3.0947\,[-0.0185/+0.0488]$ km amsl. A close-up of the source location and the error bars is shown in Fig. 10 (bottom).

For the observed $s_{\phi min} = 0.0182$ rad , $R_0 = 0.0100$ (7), which shows that the observed standard deviation is much too small for the phase distribution to be uniform.

The probabilities for random occurrence p_0 within $\pm q s_{\phi min}$ of the mean value for various values of q in (8), and the corresponding confidence levels, both from the Chebyshev inequality and from a Normal distribution, are shown in Table 3. In particular, the probability of random phase occurrence within $\pm 3 s_{\phi min}$ is an extremely small $p_0 = 1.584 \bullet 10^{-9}$. With a substantial level of confidence, the probabilities of random occurrence are extremely small, thus supporting our supposition of the existence of a localized source.

3.2. All tremor locations

We were able to locate 20 tremor sources and their locations are shown in Table 4 and Fig. 11. The plan view of Fig. 11 (top left) shows epicenters are clustered about 1.4 to 2.5 km East of the crater, and E-W (bottom) and N-S (top right) cross-sections show that the tremor sources

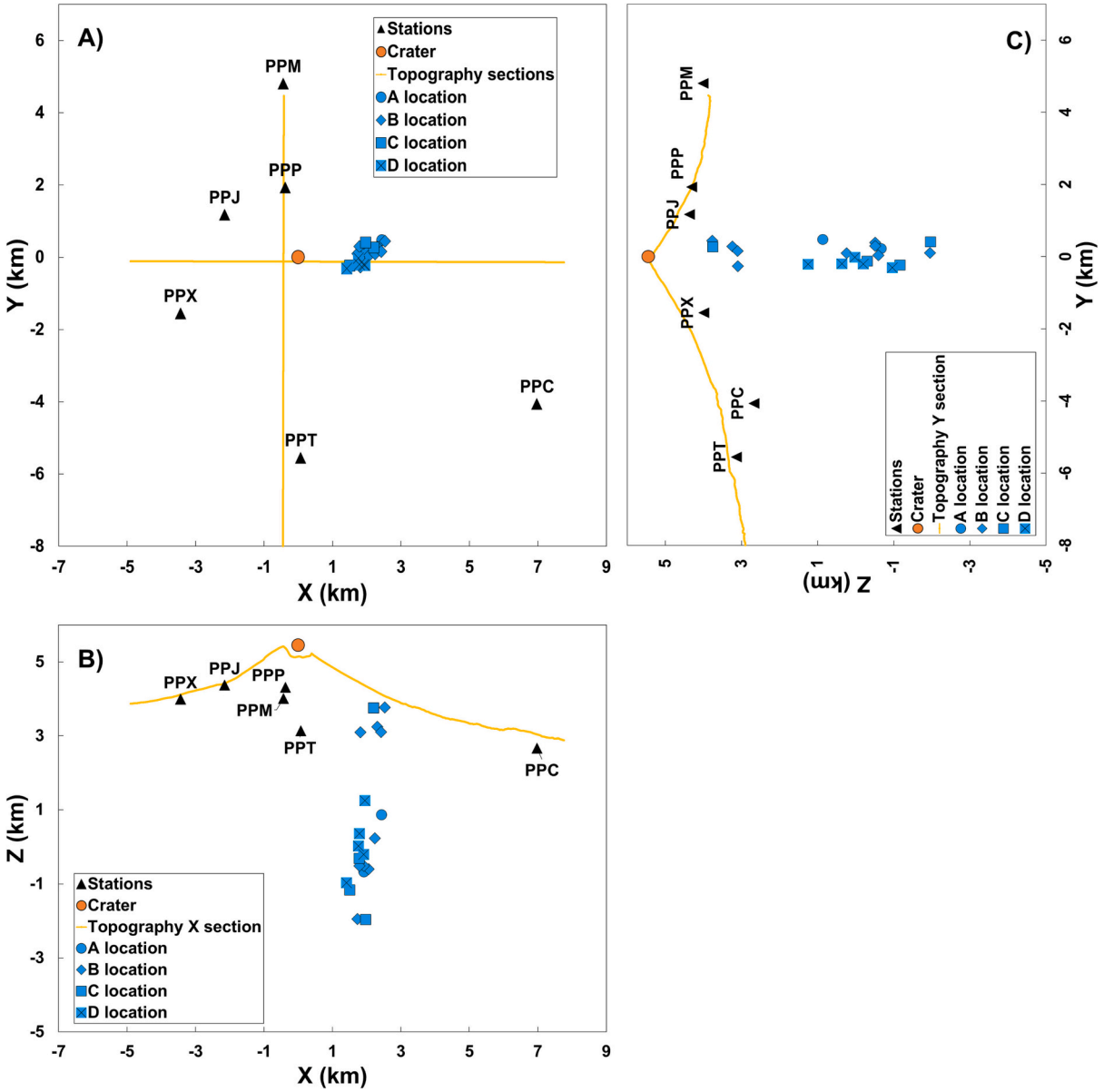

Fig. 11. Tremor source locations. Plan view (A), showing as green lines the location of the topography sections: Z vs. X (B) and Z vs. Y (C). Different symbols indicate location qualities. (For interpretation of the references to colour in this figure legend, the reader is referred to the web version of this article.)

are roughly vertically aligned. Although this alignment could be partly due to uncertainties in depth determination, its depth range of about 5 km suggests that it might have a significant component corresponding to some feature within the volcanic edifice that was active during the time when tremor was recorded.

Fig. 12 shows the evolution of the tremor activity in time, in terms of source coordinates. There is no clear trend of the parameter values with time, except for z_o, which seems to stabilize around 0 km amsl as the time of the July 25 explosion approaches; unfortunately, locations between days 15 and 21 are unreliable, but two excellent locations before and after the explosion suggest that this preferred depth may be correct.

Although a sample of twenty locations is too small to draw solid statistical results, we will mention a couple of observations. There is no correlation between source elevation z_o and frequency f_o, which means that the driving mechanism that determines the frequency can operate similarly at different depths, and suggests a mechanism such as degassing instead of resonance. There is a slight correlation between the average velocity V and z_o (Pearson's $r = 0.4716$), which agrees quite well with the velocity anomalies found by Kuznetsov and Koulakov (2014) and Berger et al. (2011b).

3.3. Locations and the array

Figs. 2 and 11 show that the station coverage is not symmetric around the epicentral clustering locations, so it is essential to see how this asymmetric station distribution might influence the source locations. To this end, we generated synthetic phase sets for the station array and located them using the same method used for locating the real data. Two sets of data were generated: set S_1 with epicenters corresponding to those found for real data and, for comparison, another set S_2 with epicenters located on the other side of the crater, where station coverage is better.

For noiseless synthetic data the location scheme works perfectly and finds the correct locations independently on where the synthetic sources were positioned with respect to the station array.

Next, noise was introduced by adding to the synthetic phases

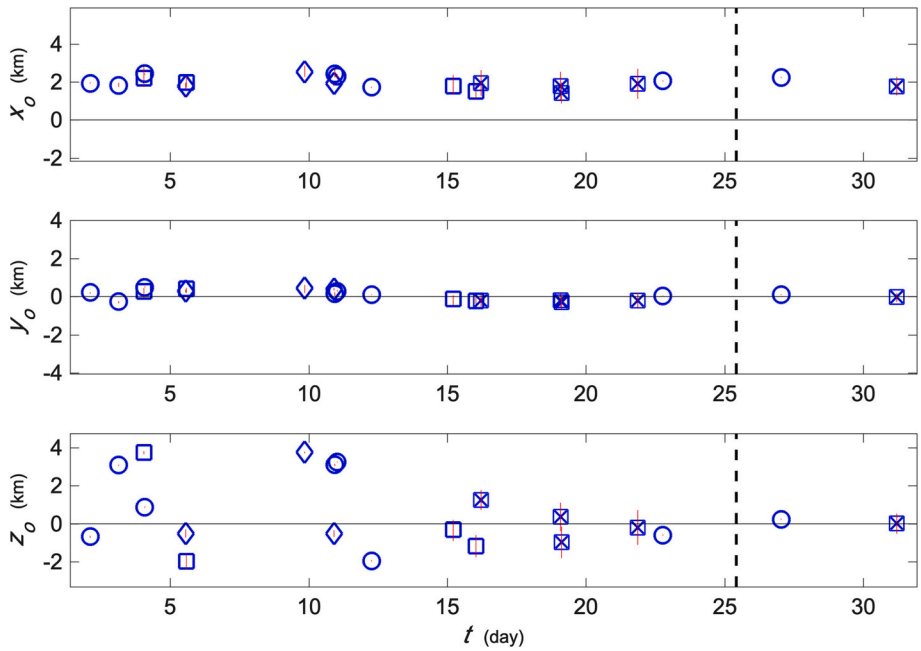

Fig. 12. Variation of the source coordinates with time, using the same conventions as in Fig. 8 and all drawn to same scale. The vertical dashed line indicates the time of the July 25 explosion.

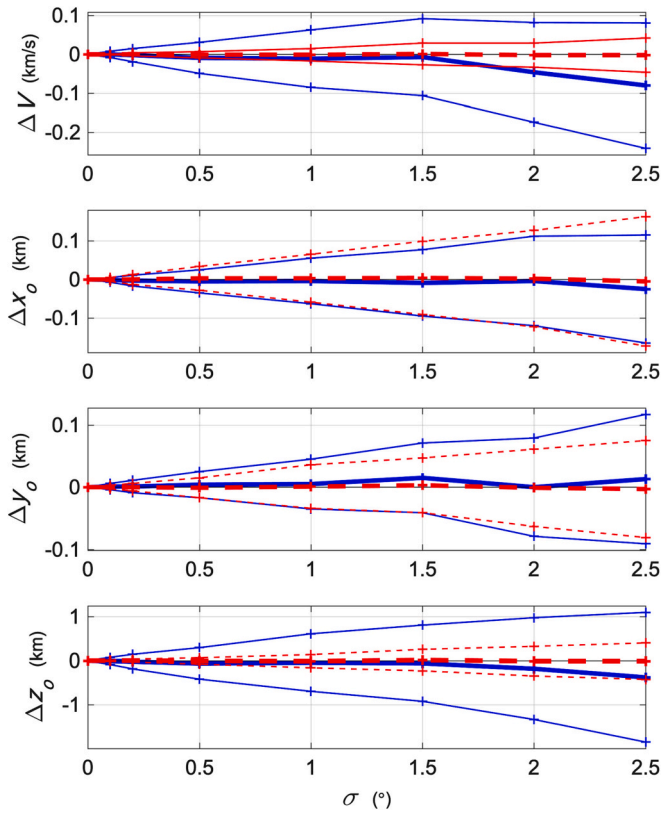

Fig. 13. Changes in the optimal velocity and location of synthetic tremor phases vs. noise from 100 realizations at each noise level. Blue lines indicate results for S_1, and red lines for S_2. Thick lines correspond to mean values, and thin lines are the means plus/minus one standard deviation. (For interpretation of the references to colour in this figure legend, the reader is referred to the web version of this article.)

normally distributed random phase shifts with zero mean and different standard deviations. The changes in location caused by adding noise are shown in Fig. 10, as thick lines for the mean variations of 100 synthetic phase sets each, and thin lines representing plus/minus one standard deviation around the mean. It should be mentioned that, unlike large sets of random numbers, sets of six random variations, one for the phase at each station, having the same standard deviation, can differ greatly from each other and result in phase sets very different from the original

Fig. 13 shows that, as expected, standard deviations increase with σ, but while V changes substantially for noise with $\sigma > 1.5°$ for S_1, the means of the location coordinates for both S_1 and S_2 vary surprisingly little.

It is clear that with standard deviations <0.2 km for x_o and ~ 0.1 km for y_o for large σ, the real epicentral locations cannot differ significantly from the ones obtained here. As would be expected, source depth is the least reliable result and, while means are not very different for S_1 and S_2, uncertainties are indeed larger for S_1 so that source determinations for phase sets having considerable noise could have errors reaching ~1.5 km.

4. Discussion

We have proposed a new method for localizing the source of harmonic tremor. The method is based on the following premises:

- The source is localized enough to be adequately modeled as a point in space.
- The tremor signal propagates radially from the source.
- The average velocity between source and seismic stations can be adequately represented by a constant value.

The method is also based on the assumption that, given the premises, the phase at the source should be the same when computed from the phase at each station and the distance to it.

Our method could be considered similar to those methods using interstation arrival times obtained from correlation (Haney, 2010; Droznin et al., 2015; Li et al., 2017; Métaxian et al., 2002; Yukutake et al., 2017) or from semblance (Furumoto et al., 1990, 1992), but while these have the disadvantage of not having an origin time, our method

has a reference point in the condition that origin phase determinations from different stations should be equal, which gives it a solid support for locating by minimizing the origin phase estimations spread.

Limitations of the method are:

a) It is essential that the time series section span an interval corresponding to an integer number of the particular dominant period used for location, which requires the spectral content of the signal to be constant over times corresponding ideally to three or more of the periods to be used.
b) Dominant periods should be long enough so that the corresponding wavelengths are larger than the source to station distances.
c) The station distribution need not be a dense array completely covering or surrounding the epicentral area, but reliable locations require a minimum of four stations distributed reasonably well around and not very far from the epicentral area.

Due to these limitations, this method of tremor source location cannot be applied to all volcanic tremor episodes; but when applicable it constitutes a new tool that can contribute to the evaluation of the internal state of a volcano.

Whether the premises and method are valid, and to what extent, is judged from application of the method to real tremor data from Popocatépetl volcano, which gives very satisfactory results that have extremely low probabilities of being due to chance; i.e., the assumptions appear to be valid and the location method works very well. Although due to the limitations of the assumptions the locations cannot be expected to be exact, their epicentral grouping and vertical alignment cannot be explained as location uncertainties and constitute a real feature of Popocatépetl's activity.

Now, let us consider how our results check with results from other studies of the Popocatépetl's activity, taking into account that these other studies do not refer to the tremor episode we studied.

The locations of our sources roughly agree with the approximate locations by Arámbula-Mendoza (2002) and Arámbula-Mendoza and Valdéz-González (2002) of tremors that occurred in November 2000, but our sources are shallower, slightly more easterly, and more aligned, although the alignment could be due to the station distribution.

Our tremor source locations coincide with regions of high V_P/V_S ratio and high velocity anomalies found by Kuznetsov and Koulakov (2014) in the structure of Popocatépetl volcano, which they suggest are due to the presence of cracks and pores containing melts and fluids revealing a fracture zone that serves as a feeding conduit for the volcano

Lermo-Samaniego et al. (2006) found two clusters of volcano-tectonic earthquakes that occurred during 1994–1997; the cluster they call Zone A has a shallow sub-cluster that coincides with the sites of our tremor sources. Events in this cluster feature emergent phases and varied focal mechanisms, which the authors consider could be related to fracturing processes due to rising magma. Berger et al. (2011a), using carefully relocated seismotectonic events also find two hypocenter clusters one of which coincides with our tremor source locations.

From all the above, we conclude that the method presented here results in approximate locations that are reliable enough to contribute to the knowledge about volcanic harmonic tremor.

Credit author statement

All authors contributed to the study conception and design. The first draft of the manuscript was written by F. Nava. All authors read and approved the final manuscript.

Funding

CICESE Internal Funds.

Declaration of Competing Interest

The authors have no affiliation with any organization with a direct or indirect financial interest in the subject matter discussed in the manuscript.

Data availability

Datasets related to this article can be requested from CENAPRED (https://www.cenapred.unam.mx/) or SSN (http://www.ssn.unam.mx/).

Acknowledgements

Our deep appreciation to Servicio Sismológico Nacional and CENAPRED for use of their data, particularly to José Castelán Pescina. We are grateful to Antonio Mendoza Camberos, Luis Yegres, and José Mojarro for technical support. This research was partially funded by CONAHCYT project 222795 and by the CONAHCYT *Investigadoras e Investigadores por México* program, project 2602. Our thanks to two anonymous reviewers (particularly to Reviewer 1) and to the editor Diana Roman for constructive criticism and helpful comments.

References

Almendros, J., Abella, R., Mora, M., Lesage, P., 2014. Array analysis of the seismic wavefield of long-period events and volcanic tremor at Arenal volcano, Costa Rica. J. Geophys. Res. Solid Earth 119, 5536–5559. https://doi.org/10.1002/2013JB010628.

Arámbula-Mendoza, R., 2002. Interpretación del tremor armónico registrado en el volcán Popocatépetl durante la crisis eruptiva de diciembre del 2000. B.E. Thesis. UNAM, Mexico.

Arámbula-Mendoza, R., Valdéz-González, C., 2002. Interpretación del tremor armónico registrado en el volcán Popocatépetl durante la actividad eruptiva de diciembre del 2000. GEOS 22, 399.

Arámbula-Mendoza, R., Valdés-González, C., Varley, N., Reyes-Pimentel, T.A., Juárez-García, B., 2016. Tremor and its duration-amplitude distribution at Popocatépetl volcano, Mexico. Geophys. Res. Lett. 43, 8994–9001. https://doi.org/10.1002/2016GL070227.

Arciniega-Ceballos, A., Chouet, B., Dawson, P., 2003. Long-period events and tremor at Popocatepetl volcano (1994-2000) and their broadband characteristics. Bull. Volcanol. 65, 124–135. https://doi.org/10.1007/s00445-002-0248-8.

Battaglia, F., 2007. Metodi di previsione statistica. Springer-Verlag, Milano.

Battaglia, J., Aki, K., 2003. Location of the seismic events and eruptive fissures on the Piton de la Fournaise volcano using seismic amplitudes. J. Geophys. Res. 108 (B8), 2364. https://doi.org/10.1029/2002JB002193.

Battaglia, J., Got, J.L., Okubo, P., 2003. Location of long-period events below Kilauea Volcano using seismic amplitudes and accurate relative relocation. J. Geophys. Res. Solid Earth 108 (B12).

Battaglia, J., Aki, K., Ferrazzini, V., 2005. Location of tremor sources and estimation of lava output using tremor source amplitude on the Piton de la Fournaise volcano:1. Location of tremor sources. J. Volcanol. Geotherm. Res. 147, 268–290.

Berger, P., Nava, F., Valdés, C., Martínez, A., 2011a. New locations of volcano-tectonic earthquakes under Popocatépetl volcano applying a genetic search algorithm. Geofis. Int. 50, 319–340.

Berger, P., Got, J., Valdés, C., Monteiller, V., 2011b. Seismic tomography at Popocatépetl volcano, México. J. Volcanol. Geotherm. Res. 200, 234–244.

Cabral-Cano, E., Correa-Mora, F., Meertens, C., 2008. Deformation of Popocatepetl volcano using GPS: Regional geodynamic context and constrains on its magma chamber. J. Volcanol. Geotherm. Res. 170, 24–34.

CENAPRED, 1995. Volcán Popocatépetl. Estudios realizados durante la crisis de 1994–1995. Secretaría de Gobernación, Sistema Nacional de Protección Civil, Centro Nacional de Prevención de Desastres. Universidad Nacional Autónoma de México, Mexico, p. 339.

Chouet, B., 2003. Volcano Seismology. Pure Appl. Geophys. 160, 739–788, 0033–4553/03/040739–50.

Chouet, B., Matoza, R., 2013. A multi-decadal view of seismic methods for detecting precursors of magma movement and eruption. J. Volcanol. Geotherm. Res. 252, 108–175.

Chouet, B., Saccorotti, G., Martini, M., Dawson, P., De Luca, G., Milana, G., Scarpa, R., 1997. Source and path effects in the wave fields of tremor and explosions at Stromboli volcano, Italy. J. Geophys. Res. 102 (B7), 15129–15150.

Chouet, B., Dawson, P., Arciniega-Ceballos, A., 2005. Source mechanism of Vulcanian degassing at Popocatépetl volcano, Mexico, determined from waveform inversion of very long period signals. J. Geophys. Res. 110, B07301. https://doi.org/10.1029/2004JB003524.

De-la Cruz-Reyna, S., Quezada, J., Peña, C., Zepeda, O., Sánchez, T., 1995. Historia de la actividad del Popocatépetl (1354-1995). In: Volcán Popocatépetl estudios realizados

durante la crisis de 1994–1995: México, D.F. Secretaria de Gobernación, Sistema Nacional de Protección Civil, Centro Nacional de Prevención de Desastres, Universidad Nacional Autónoma de México, pp. 3–22.
Delgado, H., De la Cruz, S., Tilling, R., 2008. The 1994-present eruption of Popocatépetl volcano: Background, current activity, and impacts. J. Volcanol. Geotherm. Res. 170, 1–4.
Di Grazia, G., Falsaperla, S., Langer, H., 2006. Volcanic Tremor location during the 2004 Mount Etna lava effusion. Geophys. Res. Lett. 33, L04304. https://doi.org/10.1029/2005GL025177.
Droznin, V., Shapiro, N., Droznina, Ya, Senyukov, L., Chebrov, V., Gordeev, E., 2015. Detecting and locating volcanic tremors on the Klyuchevskoy group of volcanoes (Kamchatka) based on correlations of continuous seismic records. Geophys. J. Int. 203 (1001), 1010.
Eibl, E., Lokmer, I., Bean, C.J., Akerlie, E., Vogfjörd, K., 2015. Helicopter vs. volcanic tremor: Characteristic features of seismic harmonic tremor on volcanoes. J. Volcanol. Geotherm. Res. 304, 108–117.
Espinasa, R., 2012. Historia de la actividad del volcán Popocatépetl, 17 años de erupciones. CENAPRED (Centro Nacional de Prevención de Desastres).
Espíndola, J., Godinez, M., Espíndola, V., 2004. Models of Ground Deformation and Eruption Magnitude from deep source at Popocatepetl Volcano, Central Mexico. Nat. Hazards 31, 191–207.
Furumoto, M., Kunimoto, T., Inoue, H., Yamada, I., Yamaoka, K., Akami, A., Fukao, Y., 1990. Twin sources of high-frequency volcanic tremor of Izu-Oshima volcano, Japan. Geophys. Res. Lett. 17, 25–27.
Furumoto, M., Kunimoto, T., Inoue, H., Yamaoka, K., 1992. Seismic image of the volcanic tremor source at Izu-Oshima volcano, Japan. In: Gasparini, P., Scarpa, R., Aki, K. (Eds.), Volcanic Seismology, Volume Proc. Volcanol, 3. IAVCEI, pp. 201–211.
Goldstein, P., Chouet, B., 1994. Array measurements and modeling of sources of shallow volcanic tremor at Kilauea volcano, Hawaii. J. Geophys. Res. 99 (B2), 2637–2652.
Gottschämmer, E., Surono, I., 2000. Locating tremor and shock sources recorded at Bromo volcano. J. Volcanol. Geotherm. Res. 101, 199–209.
Haney, M., 2010. Location and mechanism of very long period tremor during the 2008 eruption of Okmok Volcano from interstation arrival times. J. Geophys. Res. 115, B00B05 https://doi.org/10.1029/2010JB007440.
Hellweg, M., 2000. Physical models for the source of Lascar's harmonic tremor. J. Volcanol. Geotherm. Res. 101, 183–198.
Hotovec, A., Prejean, S., Vidale, J., Gomberg, J., 2013. Strongly gliding harmonic tremor during the 2009 eruption of Redoubt Volcano. J. Volcanol. Geotherm. Res. 259, 89–99.
Julian, B., 1994. Volcanic tremor: nonlinear excitation by fluid flow. J. Geophys. Res. 99 (B6), 11859–11877.
Konstantinou, K., Schlindwein, V., 2003. Nature, wavefield properties and source mechanism of volcanic tremor: a review. J. Volcanol. Geotherm. Res. 119 (1), 161–187.
Kumagai, H., Nakano, M., Maeda, T., Yepes, H., Palacios, P., Ruiz, M., Arrais, S., Vaca, M., Molina, I., Yamashima, T., 2010. Broadband seismic monitoring of active volcanoes using deterministic and stochastic approaches. J. Geophys. Res. 115, B08303. https://doi.org/10.1029/2009JB006889.
Kumagai, H., Londoño, J., Maeda, Y., Acevedo, A.E.R., 2019. Amplitude source location method with depth dependent scattering and attenuation structures: Application at Nevado del Ruiz volcano, Colombia. J. Geophys. Res. Solid Earth 124 (11), 11585–11600. https://doi.org/10.1029/2019JB018156.
Kuznetsov, P., Koulakov, I., 2014. The three-dimensional structure beneath the Popocatépetl volcano (Mexico) based on local earthquake tomography. J. Volcanol. Geotherm. Res. 276, 10–21.
Lees, J., Gordeev, E., Ripepe, M., 2004. Explosions and periodic tremor at Karymsky volcano, Kamchatka, Russia. Geophys. J. Int. 158, 1151–1167.
Lermo-Samaniego, J., Antayhua-Vera, Y., Chavacán-Ávila, M., 2006. Análisis de la actividad sísmica en el volcán Popocatépetl (México) durante el periodo 1994-1997. Bol. Soc. Geol. Mex. 58, 253–257.
Lesage, P., Mora, M., Alvarado, G., Pacheco, J., Métaxian, J., 2006. Complex behavior and source model of the tremor at Arenal volcano, Costa Rica. J. Volcanol. Geotherm. Res. 157 (1–3), 49–59.
Li, K., Sadeghisorkhani, H., Sgattoni, G., Gudmundsson, O., Roberts, R., 2017. Locating tremor using stacked products of correlations. Geophys. Res. Lett. 44, 3156–3164. https://doi.org/10.1002/2016GL072272.
Macías, J., Carrasco, G., Siebe, C., 1995. Zonificación de peligros volcánicos del Popocatépetl. In: Volcán Popocatépetl estudios realizados durante la crisis de 1994–1995: México, D.F. Secretaría de Gobernación, Sistema Nacional de Protección Civil, Centro Nacional de Prevención de Desastres, Universidad Nacional Autónoma de México, pp. 79–92.
Maher, S., Dawson, P., Hotovec-Ellis, A., Thelen, W., Jolly, A., Bennington, N., Chang, J., Dotray, P., 2023. Characterizing and locating seismic Tremor during the 2022 eruption of Mauna Loa Volcano, Hawai'i, with Network Covariance. Seismic Record 3 (3), 228–238. https://doi.org/10.1785/0320230020.
Maryanto, S., Iguchi, M., Tameguri, T., 2008. Constraints on the source mechanism of harmonic tremors based on seismological, ground deformation, and visual observations at Sakurajima volcano, Japan. J. Volcanol. Geotherm. Res. 170 (3–4), 198–217.
McNutt, S., 2005. Volcanic seismicity. Annu. Rev. Earth Planet. Sci. 2005 (32), 461–491. https://doi.org/10.1146/annurev.earth.33.092203.122459.
Métaxian, J., Lesage, P., 1997. Permanent tremor of Masaya Volcano, Nicaragua: wave field analysis and source location. J. Geophys. Res. 102 (B10), 22529–22545.
Métaxian, J., Lesage, P., Valette, B., 2002. Locating sources of volcanic tremor and emergent events by seismic triangulation: application to Arenal volcano, Costa Rica. J. Geophys. Res. 107 (B10), 2243. https://doi.org/10.1029/2001jB000559.
Neuberg, J., Luckett, R., Ripepe, M., Braun, T., 1994. Highlights from a seismic broadband array on Stromboli volcano. Geophys. Res. Lett. 21, 749–752.
Ogiso, M., Yomogida, K., 2012. Migration of tremor locations before the 2008 eruption of Meakandake Volcano, Hokkaido, Japan. J. Volcanol. Geotherm. Res. 217, 8–20 (D).
Ogiso, M., Yomogida, K., 2020. Estimation of relative source locations from seismic amplitude: application to earthquakes and tremors at Meakandake volcano, eastern Hokkaido, Japan. Earth Plan. Space 73, 1–14.
Ogiso, M., Matsubayashi, H., Yamamoto, T., 2015. Descent of tremor source locations before the 2014 phreatic eruption of Ontake volcano, Japan. Earth Plan. Space 67 (1), 206. https://doi.org/10.1186/s40623- 015-0376-y.
Roman, D., 2017. Automated detection and characterization of harmonic tremor in continuous seismic data. Geophys. Res. Lett. 44, 6065–6073. https://doi.org/10.1002/2017GL073715.
Rost, S., Thomas, C., 2002. Array seismology: methods and applications. Rev. Geophys. 40 (3), 1–2.
Rowe, C., Aster, R., Kyle, P., Schlue, J., 1998. Broadband recording of strombolian explosions and associated very-long-period seismic signals on Mount Erebus volcano, Ross Island, Antartica. Geophys. Res. Lett. 25, 2297–2300.
Shelly, D., Beroza, G., Ide, S., Nakamula, S., 2006. Low-frequency earthquakes in Shikoku, Japan, and their relationship to episodic tremor and slip. Nature 442 (7099), 188–191.
Siebe, C., Abrams, M., Macías, J., 1995. Derrumbes gigantes, depósitos de avalancha de escombros y edad del actual cono del volcán Popocatépetl. In: Volcán Popocatépetl estudios realizados durante la crisis de 1994–1995: México, D.F. Secretaría de Gobernación, Sistema Nacional de Protección Civil, Centro Nacional de Prevención de Desastres, Universidad Nacional Autónoma de México, pp. 195–220.
Siebe, C., Abrams, M., Macias, J., Obenholzner, J., 1996. Repeated volcanic disasters in Prehispanic time at Popocatépetl, Central Mexico: past key to the future? Geology 24, 399–402.
Soubestre, J., Seydoux, L., Shapiro, N.M., Rosnyde, J., Droznin, D.V., Droznina, S.Y., Senyukov, S.L., Gordeev, E.I., 2019. Depth migration of seismovolcanic tremor sources below the Klyuchevskoy volcanic group (Kamchatka) determined from a network-based analysis. Geophys. Res. Lett. 46 (14), 8018–8030. https://doi.org/10.1029/2019GL083465.
Unglert, K., Jellinek, A., 2015. Volcanic tremor and frequency gliding during dike intrusions at Kı¯lauea—a tale of three eruptions. J. Geophys. Res. Solid Earth 120 (2), 1142–1158.
Valdés, C., González, G., Arciniega, A., Guzmán, M., Nava, E., Gutierrez, C., Santoyo, M., 1995. Sismicidad del volcán Popocatépetl a partir del 21 de diciembre de 1994 al 30 de marzo de 1995. In: Volcán Popocatépetl estudios realizados durante la crisis de 1994–1995: México, D.F. Secretaría de Gobernación, Sistema Nacional de Protección Civil, Centro Nacional de Prevención de Desastres, Universidad Nacional Autónoma de México, pp. 129–138.
Wassermann, J., 1997. Locating the sources of volcanic explosions and volcanic tremor at Stromboli volcano (Italy) using beam-forming on diffraction hyperboloids. Phys. Earth Planet. Inter. 104, 217–281.
Wech, A., Creager, K., 2008. Automated detection and location of Cascadia tremor. Geophys. Res. Lett. 35 (L20302), 2008. https://doi.org/10.1029/2008GL035458.
Yukutake, Y., Honda, R., Harada, M., Doke, R., Saito, T., Ueno, T., Sakai, S., Morita, Y., 2017. Analyzing the continuous volcanic tremors detected during the 2015 phreatic eruption of the Hakone volcano. Earth Plan. Space 69, 164.